Nano Energy 73 (2020) 104809

Contents lists available at ScienceDirect

Nano Energy

journal homepage: http://www.elsevier.com/locate/nanoen

A water droplet-powered sensor based on charge transfer to a flow-through front surface electrode

L.E. Helseth

Department of Physics and Technology, Allegaten 55, 5020, Bergen, University of Bergen, Norway

ARTICLE INFO

Keywords:
Water droplet
Triboelectric nanogenerator
Sensor
Current
Polymer

ABSTRACT

A water droplet sensor based on a flow-through front surface electrode is demonstrated. It is shown that a triboelectric nanogenerator based on a metal-dielectric junction can be utilized to construct simple, self-powered water drop counters that require only a minimum of electronical components. Every water drop generates a flash in a light emitting diode, which is detected by a silicon photodetector located some distance away. Different transducer designs are investigated, either in the form of flat tilted surfaces or polymer-covered metal wires, with the former found to provide the largest charge transfer while the latter is less sensitive to positional stability. It is also demonstrated that the sensor could be utilized to monitor the state of the magnetic field-controlled turbidity of a solution without any additional electronics, thus making a minimalistic design feasible.

1. Introduction

It is well-known that water acquires electrical charge when coming in contact with solid surfaces, and that this can be used to generate electrical currents [1]. However, as the understanding of the process has progressed, the recent few years has seen a range of new self-powered sensors and actuators based on contact electrification of water droplets [2–7]. The integration of such water-droplet triboelectric nanogenerators in solar cells [8–14] or wearable items [15,16] has become important. The development of materials for water drop energy harvesting is closely interwoven with those developed for water wave energy harvesting [16–22], since both rely on water/solid/air interfaces. The development of suitable dielectric materials has been guided by the properties of the surface, including hierarchical structure [6,8,10,12–15,23–28], slippery and lubricant-impregnated porous surfaces [29,30] as well as biomimetic [31] and natural materials [32,33]. A range of parameters influencing surface energy are known to influence the charge transfer [34–37], and the use of charge supplies [38] or electret precharging [39] allows performance enhancement. Also, the droplet impact dynamics plays a significant role [40,41], which makes it a real challenge to find the optimal combination of surface properties for best performance. The water droplets can either be dropped, pumped, splashed or slapped, impacting on single, interdigital or other complicated electrode structures, where the latter allows the harvested energy to be increased [8,15,42–47].

The picture is further expanded by the fact also air bubbles in water can be used to harvest energy [48,49]. The recent demonstration that droplets falling though liquid membranes also allow charge transfer can be used to open up new applications [50]. Redox-induced electricity using water droplets may further aid the development of self-powered wearable electronics [51].

The fact that liquids coming in contact with common polymers allow charge transfer has been used to develop different types of sensors [52–55] and actuators [56]. Light distress and communications signals and by emission of light has been investigated [57,58]. An optical switch driven by a triboelectric generator was presented in Refs. [59]. Different designs for monitoring liquids could involve, e.g., mechanically active transducer elements utilizing solid gas or solid-water interaction [60–62], while rotary disc-shaped triboelectric nanogenerators have been developed for online monitoring of ion concentration [63]. Liquid-solid interactions may allow rapid and accurate liquid leakage detection [64].

In the current work I investigate a new type water drop energy harvesting system based on the idea of a front-electrode coming in contact with water as presented for water waves in Ref. [22] and water droplets in Refs. [7]. Also, in Ref. [65] a front-surface electrode was used, but with the goal to investigate the charge transfer coefficient for water droplets. As opposed to previous studies, the front electrode used in the current study is a flow-through type, which allows some additional freedom in creating devices for new environments, including funnels and spill guards. I elucidate the theoretical working mechanism of the design, and show how it can be used to detect individual water

E-mail address: Lars.Helseth@ift.uib.no.

https://doi.org/10.1016/j.nanoen.2020.104809
Received 17 March 2020; Received in revised form 4 April 2020; Accepted 4 April 2020
Available online 18 April 2020

droplets or monitor the turbidity of a solution.

2. Background and working mechanism

When hydrophobic fluoropolymer surfaces come in contact with water, negative charge may develop. Considerable amounts of research have been conducted in order to understand the underlying mechanisms, both from theoretical and experimental points of view [65–72]. While there is evidence suggesting that the negative charge occurs due to preferential adsorption and/or orientation of O–H groups, and there is significant recent progress revealing the influence of contact line movement, ion concentration and polymer side-groups [65,71,72], the basic mechanism causing the charge transfer is still not fully understood.

The sensor system studied in this work is based on water-droplet-induced charge transfer, and is illustrated in Fig. 1. It differs from that of Ref. [7] in that the front-surface electrode coming in contact with water drops is separated from the contact electrification layer, thus allowing a more flexible design but at the cost of losing some of the ability to build up charge from droplets or external ion injection.

Water drops are falling onto a fluoropolymer surface, under which an electrode is attached, see Fig. 1 b). The fluoropolymer surface is already charged negatively by previous droplets falling onto it, and a corresponding positive charge is induced in the underlying metal electrode. When the water drops hit the insulating polymer surface, some of the charge on the fluoropolymer surface is 'neutralized' by positive charge in the water droplet, thus forming an electrical double layer. Almost simultaneously, the water droplet also spreads over a porous metal electrode, thus allowing the charge to be pumped into the droplet, see Fig. 1c). Since water, even in its purest form, has a finite conductivity, this charge may contribute to the further buildup of the electrical double layer at the surface of the fluoropolymer. In a single-electrode arrangement such as that studied in e.g. Ref. [8,12,40], this charge would have not been pumped back into the droplet, but instead go directly to ground, thus reducing the contribution to the electric double layer. When the droplet has finally lost contact with the fluoropolymer, it brings along the positive charge, and a corresponding return current with opposite polarity of that shown in Fig. 1 c) will occur, see Fig. 1 d). The currents are large enough to light up an LED, and the pulsed light can be sensed by a detector, see Fig. 1a).

To further illustrate the working mechanism, finite element simulations of the triboelectric nanogenerator under open circuit potential were performed in COMSOL 5.4. The surface charge on the FEP surface was selected to be $-0.1\ \mu C/m^2$. The metal electrode covered by polymer was assumed to have a free-floating potential, whereas the electrode coming in contact with water was grounded. Due to the negative surface charge, the polymer surface is at a negative potential. As can be seen from Fig. 2, when the droplet moves over the transition from FEP to metal, the floating potential increases by about 26 V before returning to its original value when the droplet has left the polymer surface and only is in contact with the metal. Thus, one may expect to observe a positive voltage pulse of about 26 V between the two electrodes as the droplet passes. In a closed-circuit system as described in Fig. 1b) and c), the current would run from the polymer-covered electrode to the front-surface metal electrode when the latter comes in contact with the water.

3. The energy harvesting system

In order to investigate different methods for generating light pulses, three different designs were considered. In design 1 and 2, a 50 μm thick FEP film (DuPont) was glued with PDMS to a copper plate or an aluminum tape, see Fig. 3. The surface was placed approximately 45°

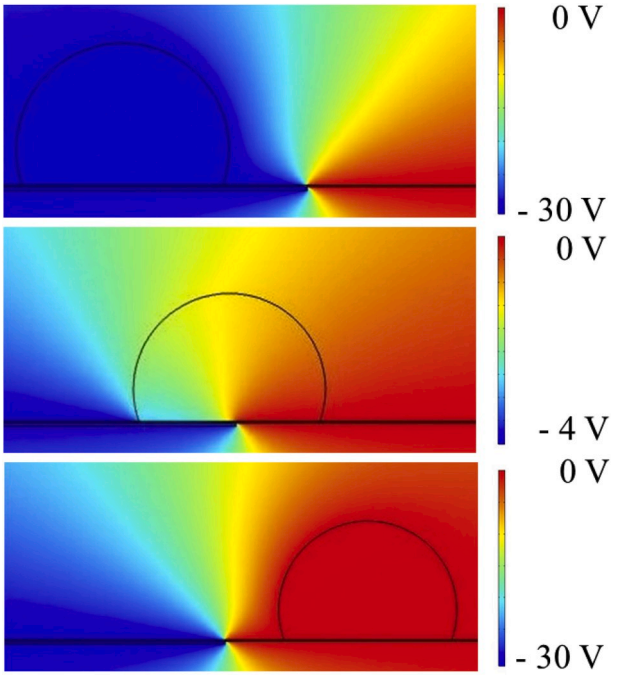

Fig. 2. Finite element simulations of the changes in electric potential as the water drop moves from left to right, transitioning from an FEP surface of surface charge $-0.1\ \mu C/m^2$ to an earthed metal surface.

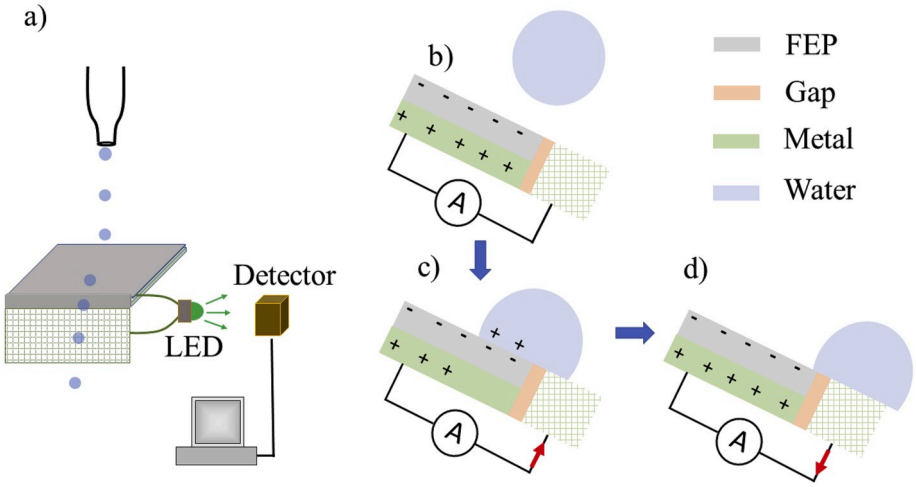

Fig. 1. The water drop sensor setup (a). In b)-d), a simplified schematic drawing of the working mechanism is presented, as explained in the text.

with the vertical line followed by falling droplets. In design 3, a 0.22 mm diameter copper wire (Block) was inserted into a 0.3 mm Teflon tube (AlphaWire), and then a length of about 0.5 m was threaded in between the hexagonal Al mesh as shown in Fig. 3. In all cases, the metal electrode to be contacted by water drops was a flow-through hexagonal aluminum mesh with hole openings of about 6 mm. Thus, while contacting the fluoropolymer surface (FEP in design 1 and 2, Teflon in design 3), the water droplets also come in contact with the aluminum mesh, and a current pulse as described in Fig. 1 occurs.

It should be pointed out that while in design 1 and 2 the water has to hit the transition between the FEP and front-surface metal electrode, thus making the useful impact region rather narrow. However, in design 3 the Teflon wire is wrapped around the aluminum mesh electrode, and the drop could therefore hit anywhere and still come into contact with both polymer and metal simultaneously. This makes design 3 less vulnerable to positioning of the device relative to the incoming water drop.

4. Electrical characterization of the energy harvesting systems

The droplets were released from a height of 18 cm, using an earthed dropper connected to a pump, see also Ref. [73]. A Keithley 6514 instrument was used to measure the closed circuit current (I_{sh}) and the open circuit voltage (V_{oc}) of the three different designs. As examples of the measured electrical parameters, Fig. 4a) and b) show the open circuit voltage and closed circuit current for 50 μL droplets impinging on the FEP-metal surface of design 1 at a rate of almost 4 droplets per second. In Fig. 4c) and d) the same electrical parameters are shown for design 3 when the droplet rate is doubled. It is noted that the open circuit voltage and closed-circuit currents are nearly tenfold reduced, most likely due to the reduced surface area (much smaller than a drop) of the Teflon wire.

In Fig. 5a) and b) the open circuit voltage and closed circuit current for 50 μL droplets impinging on the FEP-metal surface of design 2 at a rate of almost 4 droplets per second is displayed. Note that also here the electrical performance is poorer than in design 1, despite the fact that these two design utilize the same FEP film. Several different funnels were tested, and it is believed that the curvature of the funnel in design 2 might cause a reduction in the impact spreading of the droplet thereby reducing the current and voltage.

Fig. 5 c) shows a single current pulse under closed-circuit conditions. As pictured in Fig. 1 c), the droplet spreading over the polymer-metal interface results in a positive current into front-surface electrode, i.e. electrons moving into the metal electrode on the backside of the fluoropolymer. The droplet spreading across the polymer-metal interface occurs within 1–2 ms, while the subsequent unidirectional translational movement across the interface takes about 10 ms, and charge recovery is therefore considerably slower. This can be understood by noting that the spreading of the water droplet over the hydrophobic polymer is much faster than the subsequent droplet removal from the hydrophilic front-surface electrode. If one removes the connection between the back-electrode of the polymer and the front-surface hexagonal Al mesh electrode, the device functions as a single electrode triboelectric nanogenerator. The peak current is now reduced by a factor of two. It is also found that the charge transfer during the fast droplet spreading, i.e. the positive part of the current pulse in Fig. 5c) and d), is reduced from 4 nC to 2 nC, also a factor of two. This reduction is expected from the visualization in Fig. 1, since none of the charge in a single-electrode triboelectric nanogenerator is pumped back into the electrical double layer.

The current was also investigated as a function of water droplet volume for design 1, as seen in Fig. 6. In Fig. 6 a) the current pulses due to 8 μL droplets are displayed, while Fig. 6 b) shows data for 75 μL droplets. It is seen that not all the droplets produce a current pulse when the droplets are 8 μL, an effect that only becomes more pronounced for even smaller droplets. One reason for this behavior might be that small droplets are not able to clear the FEP-metal transition properly at the given kinetic energy, and may become attached to it. Moreover, it should also be pointed out that weak airflow may cause the smallest droplets to not hit the FEP-metal transition spot on, thus causing large variations in signal. Fig. 6 c) shows that the peak current grows nearly linearly with drop size. By integrating the positive current pulse to find the charge transfer during the fast droplet spreading, it is found that also the positive charge transfer scales linearly with the drop size as seen in Fig. 6 d). It should be mentioned, as discussed above, that there is also corresponding slower negative charge transfer of equal magnitude, such that the total charge in the current pulse generated by one droplet is approximately zero.

The current and voltage output presented in Figs. 5 and 6 is considerably smaller than that observed in Ref. [7], where charges of 50 nC and current peaks approaching 300 μA where reported using a fluoropolymer-metal transition in a system that was precharged by either water droplets or ion injection. In the current study there is no precharging, thus being the main reason that the transferred charges are about an order of magnitude smaller. However, it should be pointed out that the charges and currents reported here are considerably larger than the comparable currents obtained with similar materials and droplet-falling conditions using the single-electrode or interdigital electrode geometries [38,40], thus making the particular geometry investigated here interesting even without precharging. Moreover, the current design does exhibit a front-surface electrode laterally separated from the FEP electrification layer, which allows one to play around more easily with the metal electrode design as reported above.

At this point it should also be pointed out that in both design 1 and 2 the water droplets have to impact the transition between the FEP and front-surface metal electrode to generate a large signal, thus making them sensitive to position placement. To see this, Fig. 7 a) shows the short-circuit current versus time as obtained by positioning the FEP-metal junction to obtain the maximum signal from design 2 using 50 μL water droplets, whereas Fig. 7 b) shows the corresponding signal when the droplets impact 1 cm further up thus only contacting the polymer before translating to the FEP-metal junction. It can be seen that the signal is now rather sporadic, probably depending to some degree on charge accumulation of droplets near the junction. In general, the variation of current with position depends on droplet dynamics upon impact, i.e. the splashing regimes, and such a study is outside the scope of this work. However, I have established that there is always a position for droplet impact that gives maximum current signal, and that variations of about a few millimeters within this maximum position do not give significant changes in signal.

Another variable of interest is the pH, as it is known that it may influence the performance in water drop energy harvesting [71]. The black boxes in Fig. 7 c) and 7 d) show the maximum current and charge

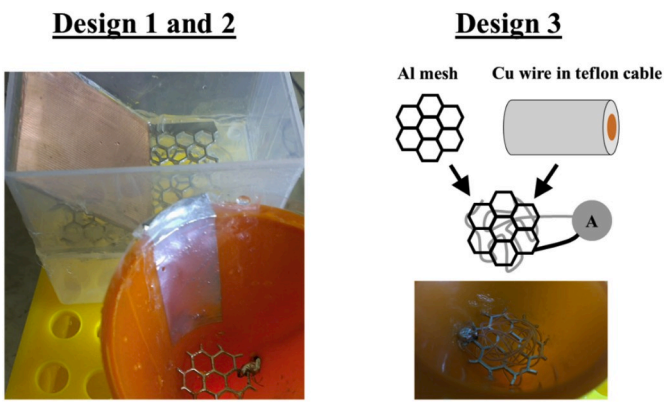

Fig. 3. Three different designs utilizing a flow-through aluminum mesh as front-surface electrode coming in contact with water combined with either FEP film on metal (design 1 and 2) or a Cu wire immersed in a hollow teflon cable (design 3). The only difference between design 1 and 2 is that a funnel is used to collect water in design 2. A funnel is also used in design 3.

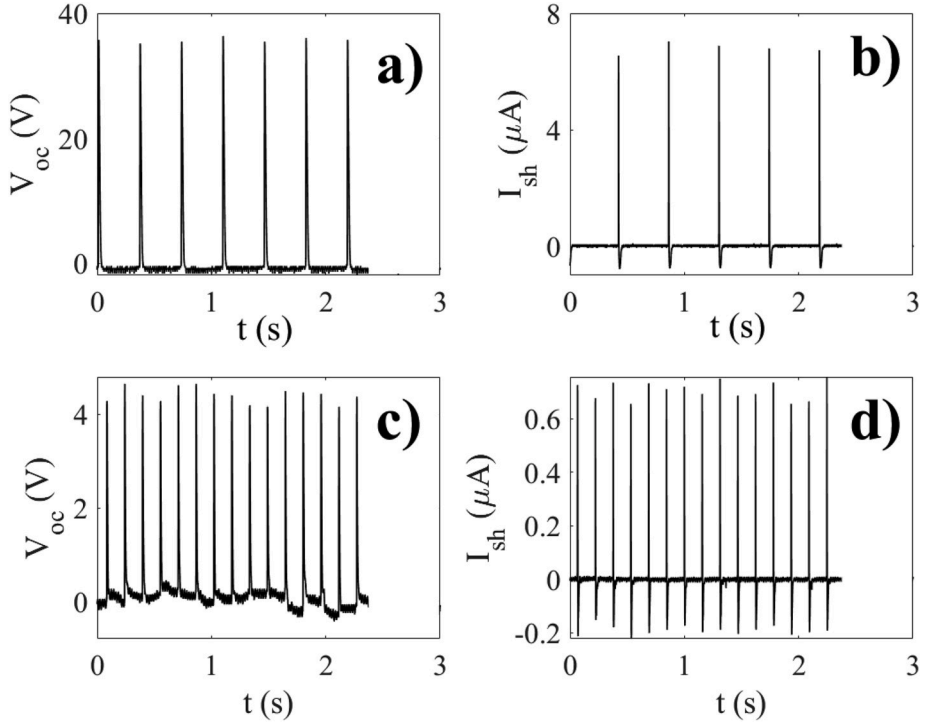

Fig. 4. The open circuit voltage (a,c) and the short circuit current (b,d) of design 1 and 3, respectively. Different drop rates were used, but that did not influence the values of the current and voltage.

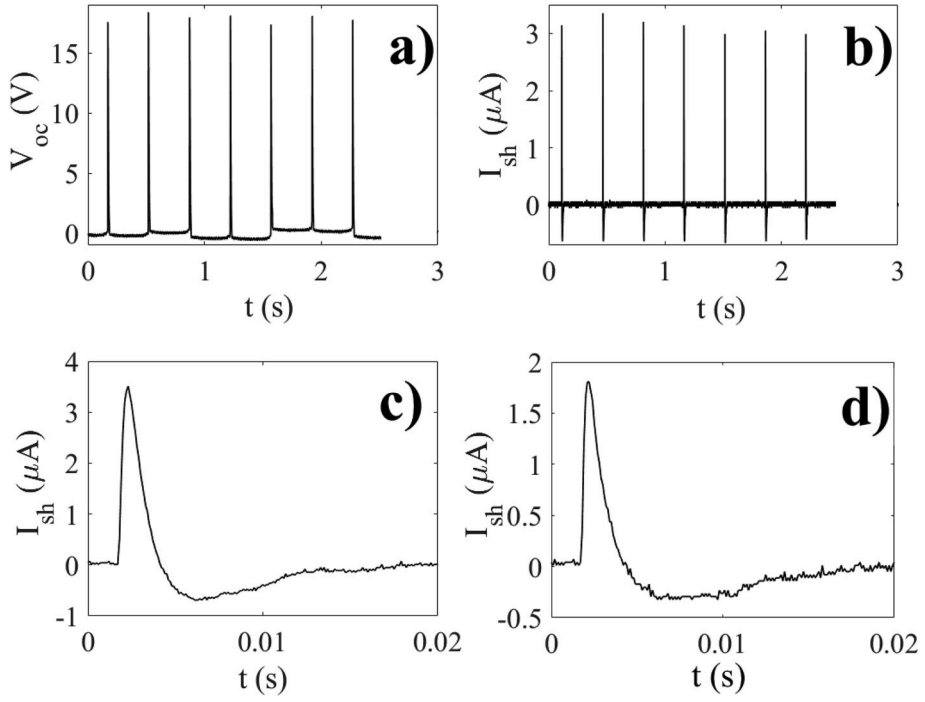

Fig. 5. The open circuit voltage (a) and the short circuit current (b) of design 2 with 50 μL water droplets. A current pulse is shown in c), whereas d) shows the corresponding current pulse if the metal interface is removed from the circuit such that the device functions as a single-electrode triboelectric nanogenerator.

when 50 μL droplets of various pH impact the metal-FEP transition of design 2. With the experimental setup used, it was found difficult to test droplets over an extended range of pH due to the copious amounts of solution and the extensive cleaning needed between each pH, so only three pH values were tested in this way. In order to be able to extend to a larger range of pH values, I decided to make a dipping device which could move the FEP-metal transition vertically across a water surface in a 70 mL cup filled with liquid. The dipping device is a FEP-metal transition very similar to that of design 1 (Fig. 3), but with the hexagonal aluminum mesh electrode replaced by a 0.03 mm thick aluminum film attached on top of the lower part of the FEP film. The device was oscillated using an electromagnetic shaker (Smart Materials GmbH),

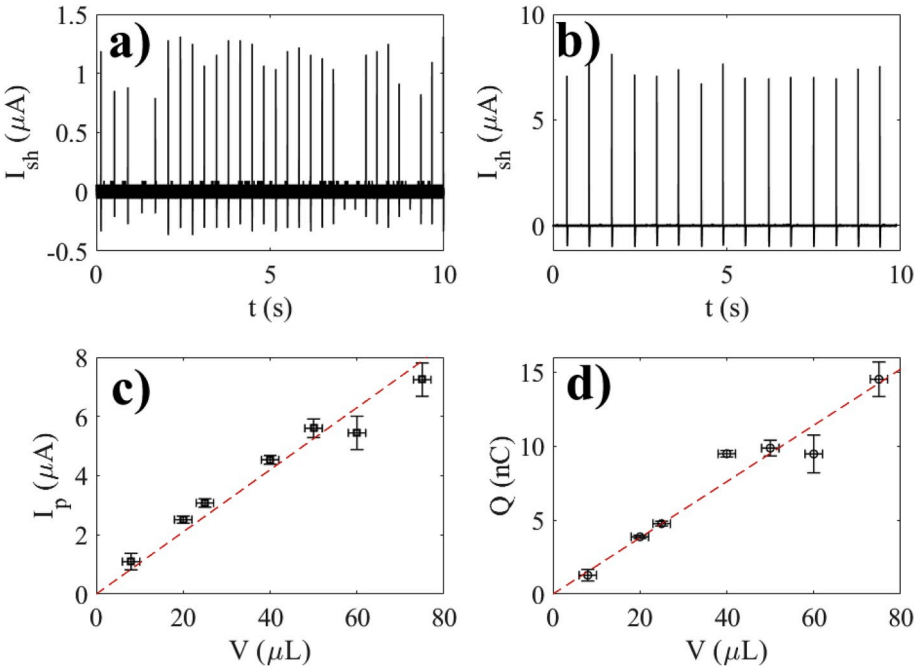

Fig. 6. The current versus time for droplets of volume 8 μL (a) and 75 μL (b) using design 1. The peak current (c) and the positive charge transfer (d) are also displayed as functions of droplet volume.

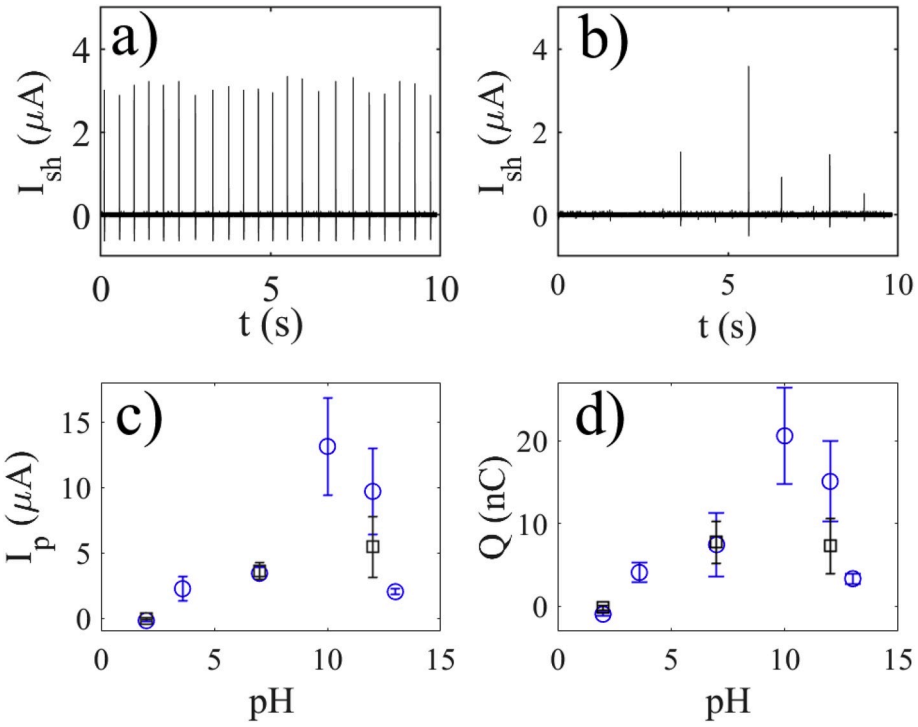

Fig. 7. The current versus time for 50 μL droplets impacting spot on (a) or 1 cm above (b) the FEP-metal transition on design 2. In c) and d), the peak current and charge are shown as a function of pH for 50 μL droplets impacting design 2 (black boxes), or the dipping device described in the text (blue circles).

also used in Ref. [39], with a frequency 5 Hz and amplitude 1 cm. In this way, the water surface in the 70 mL cup moved up and down past the FEP-metal transition. The width of the FEP-metal transition (20 mm) was made such that the current and charge matched measured matched that of design 2 as seen in Fig. 7 a). The peak current and charge as the device is dipped into water is shown as blue circles in Fig. 7c) and d), respectively. It is seen that there are significant variations in the signals, but that they do overlap with those found by dripping water droplets onto design 2, to within the experimental uncertainty. There are three interesting observations that could be made from Fig. 7 d). First, there is a maximum value of transferred charge at slightly basic pH. While the droplets impacting on design 2 appear to give rise to similar charge transfer at pH 7 and pH 12, the dipping device appears to exhibit a maximum charge transfer at pH 10. At this point, the reason for this behavior is not known, but it might be related to enhanced preferential adsorption of O–H groups, although one cannot entirely rule out

enhanced charge transfer at the metal surface. However, further study of this behavior is outside the scope of this work. As the pH increases further, the charge transfer tends to decrease again, below what is found for pure water. Moreover, it is found that the charge becomes weakly negative, about – 1 nC, for pH 2. It should be pointed out that electrokinetic measurements on polytetrafluoethylene have demonstrated that the zeta potential changes sign at pH between 3 and 4 [74]. Moreover, the observations reported in Fig. 7 d) for low and high pH's are in qualitative agreement with the observations made on a different system in Refs. [71], thus suggesting that electrification of the hydrophobic polymer controls the charge transfer in these pH ranges.

5. Water droplet sensor

A water droplet sensor was constructed by connecting the generator to a light emitting diode, as shown in Fig. 1 a). The light was received by a silicon detector (Thorlabs, PDA36A-EC), mounted in a cage system (Thorlabs) 10 cm away from the light emitting diode. The signal from the detector was recorded by an oscilloscope (Picoscope 3000) connected to a computer. In presence of ambient light, as one would expect in most practical situations, the light emitting diode signal will appear on top of some background signal, as seen in Fig. 8 a) for 50 μL droplets falling from a height of 18 cm on design 1. A close-up of the marked signal pulse in Fig. 8 a) is depicted in Fig. 8 b). Note that the signal from the energy harvester is rectified, such that only the positive pulse remains. The corresponding signals on design 2 and 3 are shown in Fig. 8 c) and 8 d), respectively. In all cases the background bias is about 25 mV, and one would need a LED current of about 0.5 μA to overcome this bias. On top of that, the noise in the detection system is about 5 mV, which means that the current peak should exceed 0.5 μA to be detected. It is seen that for the given ambient light, the current pulses from design 3 are just barely detected without failure. Indeed, as seen from Fig. 4 d) the current peaks are about 0.7–0.8 μA, which is just above the threshold limit. With design 1, which gave the largest current pulses, it was found that droplets as small as 8 μL could barely be detected by the detection system. Due to the fact that all such small droplets are not able to clear the FEP-metal transition properly at the given kinetic energy, it can be concluded that 8 μL is at the detectability limit of the current water drop sensor. Thus, with design 1 droplets with volume above 8 μL, with design 2 droplets larger than about 20 μL, whereas with design 3 only droplets of 50 μL or above could be counted individually for the given kinetic energy. Providing more kinetic energy by increasing the falling height would be one way to attempt to increase the detector signal. However, that would require a more bulky system that could not easily used indoors to detect water droplets. Testing the system in natural rain is also of interest, but that is beyond the scope of the current study.

6. Turbidity sensor

The proposed sensor system can be used to monitor the turbidity of a liquid sample given a continuous access to falling water drops. As shown in previous studies, monitoring the turbidity of liquid solutions of superparamagnetic beads allows one to determine a unidirectional magnetic field as well, and subsequently do analysis of the colloidal aggregate state to monitor the presence of e.g. biopolymers [75,76]. In this study, 10 μL carboxyl modified paramagnetic polystyrene beads of radius a = 1.4 μm (M270, Dynal) at density of 2×10^9 beads per mL were placed between the two glass plates with a spacer of about 0.1 mm. The colloids consist of nanoscale iron oxide grain in a polystyrene matrix, thus exhibiting superparamagnetic behavior [77]. The magnetic field is supplied by running a current through a coil such that the resulting magnetic field points perpendicular to the transmission cell. The magnetic field detection principle is shown in Fig. 9, where the transmission cell containing superparamagnetic beads is placed between the light emitting diode and the silicon detector. In absence of any magnetic field the colloids form a two-dimensional arrangement that blocks light, see Fig. 9 a). However, if an axial magnetic field is applied, the magnetic beads form chains and the transmittance is significantly reduced, see Fig. 9 b).

Fig. 10 a) shows the signal received by the silicon detector when the magnetic field is switched on (4 mT) or off (0 mT) over a period of 50 s. The system is now placed in complete darkness by surrounding the light emitting diode and the detector by black cardboard. It takes typically 2–3 s for the colloids to align with the magnetic field, thus determining

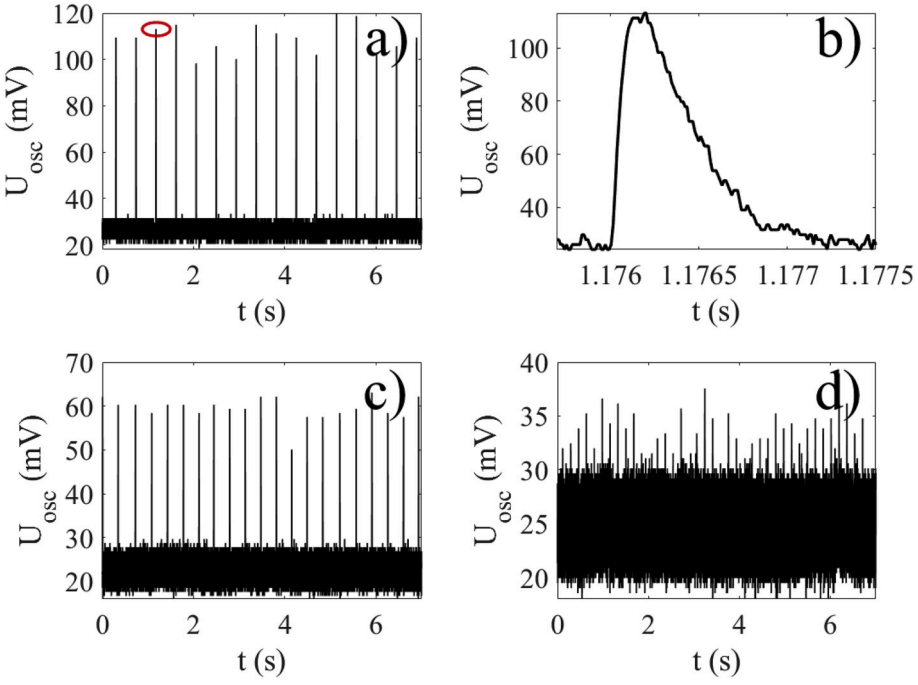

Fig. 8. The voltage U_{osc} measured over the silicon detector when a current I_{LED} is injected into the LED due to a impacting water droplets for design 1 (a,b), design 2 (c) and design 3 (d). The encircled peak in a) is the current trace shown in b).

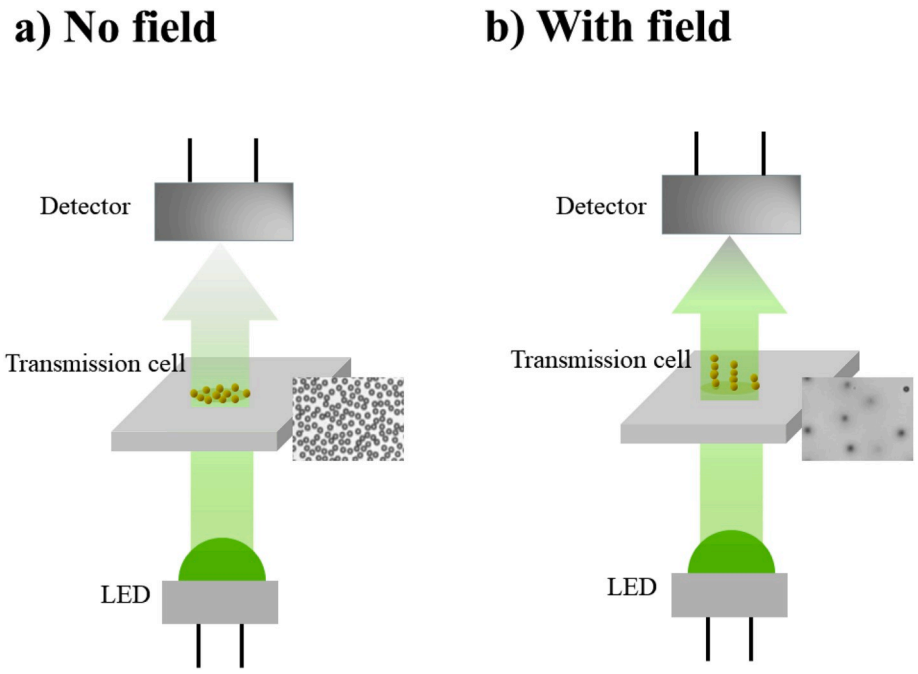

Fig. 9. The principle of a magnetic field-controlled turbidity sensor based on a droplet-powered light emitting diode.

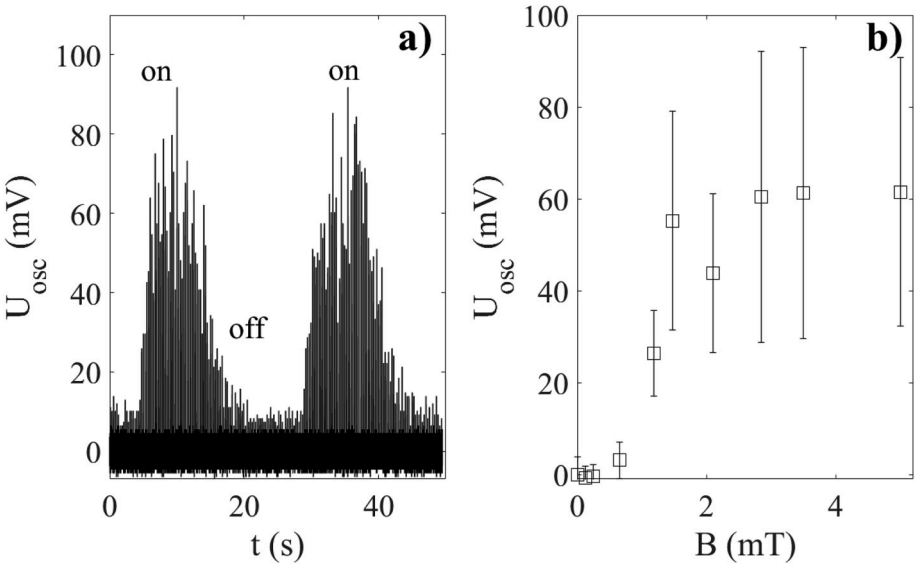

Fig. 10. The detected signal in the silicon detector when the magnetic field is turned on or off (a), and the average signal as function of magnetic field (b). The large fluctuations is due to the varying signal generated by each droplet.

the temporal response of the system.

Fig. 10 b) shows the observed average signal from the detector as a function of magnetic field B. The transition range where the colloids realign with the magnetic field is between 1 and 2 mT, and at about 2 mT, the signal is fully saturated due to full alignment. As seen in Fig. 10 a), the blinking drop detector can easily function as a two state-detector, distinguishing a fully opaque state where the colloids block much of the light from a transparent state where the light is allowed to pass the transmission cell. Due to the variations in current due to each droplet hitting the fluoropolymer-electrode transition, there are significant fluctuations of the detected signal in the silicon detector. If one wants to monitor the colloidal aggregation state more precisely, one could construct a system with a reference detector receiving some of the light before the transmission cell. Under such circumstances the variations in signal due to the variations in current from the energy harvester can be countered by normalizing the signal to that of the reference. However, this task is outside the scope of the current study.

7. Conclusion

A water droplet energy sensor based on charge transfer to a front electrode is demonstrated and the working mechanism is elucidated. The sensor system utilizes that the charge is pumped from the back electrode to the front electrode when the droplets passes the polymer-metal surface, thus allowing more charge to transfer during each droplet impact as compared to a single electrode mounted on the backside of the polymer. Different designs and applications are demonstrated. The design could apply to various types of turbidity

meters or rain collectors. Weather stations collect rain in holders that allow analog or digital readout of the water level in millimeter, either in-situ or by post-collection, thus requiring that the water passes unhindered without loss through the water collection device. However, the droplets are not individually detected in such weather stations, thus rendering the ability to extract counts of droplets or droplet size distributions a challenging task. The flow-through design presented could aid the development of such a task.

Declaration of competing interest

The authors declare that they have no known competing financial interests or personal relationships that could have appeared to influence the work reported in this paper.

CRediT authorship contribution statement

L.E. Helseth: Conceptualization, Data curation, Formal analysis, Funding acquisition, Investigation, Methodology, Project administration, Resources, Software, Supervision, Validation, Visualization, Writing - original draft, Writing - review & editing.

References

[1] W. Thomson, On a self-acting apparatus for multiplying and maintain electric charges, with applications to illustrate the voltaic theory, Proc. Roy. Soc. Lond. 16 (1867) 67–72, available at: http://www.jstor.org/stable/112474.

[2] D. Jiang, M. Xu, M. Dong, F. Guo, X. Liu, G. Chen, Z.L. Wang, Water-solid triboelectric nanogenerators: an alternative means for harvesting hydropower, Renew. Sustain. Energy Rev. 115 (2019) 109366.

[3] W. Tang, B.D. Chen, Z.L. Wang, Recent progress in power generation from water/liquid droplet interaction with solid surfaces, Adv. Funct. Mater. 29 (2019) 1901069.

[4] J.K. Moon, J. Jeong, D. Lee, H.K. Pak, Electrical power generation by mechanically modulating electrical double layers, Nat. Commun. 4 (2013) 1487.

[5] S.-H. Kwon, J. Park, W.K. Kim, Y. Yang, E. Lee, C.J. Han, S.Y. Park, J. Lee, Y.S. Kim, An effective energy harvesting method from a natural water motion active transducer, Energy Environ. Sci. 7 (2014) 3279–3283.

[6] Z.H. Lin, G. Cheng, S. Lee, K.C. Pradel, Z.L. Wang, Harvesting water drop energy by sequential contact electrification and electrostatic induction process, Adv. Mater. 26 (2014) 4690–4696.

[7] W. Xu, H. Zheng, X. Zhou, C. Zhang, Y. Song, X. Deng, M. Leung, Z. Yang, R.X. Xu, Z.L. Wang, X.C. Zeng, Z. Wang, A droplet-based electricity generator with high instantaneous power density, Nature 578 (2020) 392–396.

[8] L. Zheng, Z.H. Lin, G. Cheng, W. Wu, X. Wen, S. Lee, Z.L. Wang, Silicon-based hybrid cell for harvesting solar energy and raindrop electrostatic energy, Nano Energy 9 (2014) 291–300.

[9] Q. Liang, X. Yan, Y. Gu, K. Zhang, M. Liang, S. Liang, X. Zheng, Y. Zhang, Highly transparent triboelectric nanogenerator for harvesting water-related energy reinforced by antireflection coating, Sci. Rep. 26 (2015) 4690–4696.

[10] S.B. Jeon, D. Kim, G.-W. Yoon, J.-B. Yoon, Y.-K. Choi, Self-cleaning hybrid energy harvester to generate power from raindrop and sunlight, Nano Energy 12 (2015) 636–645.

[11] Q. Tang, H. Zhang, B. He, P. Zhang, An all-weather solar cell that can harvest energy from sunlight and rain, Nano Energy 30 (2016) 818–824.

[12] L.E. Helseth, X.D. Guo, Fluorinated ethylene propylene thin film for water droplet energy harvesting, Renew. Energy 99 (2016) 845–851.

[13] Y. Liu, N. Sun, J. Liu, Z. Wen, X. Sun, S.T. Lee, B. Sun, Integrating a silicon solar cell with a triboelectric nanogenerator via a mutual electrode for harvesting energy from sunlight and raindrops, ACS Nano 12 (2018) 2893–2899.

[14] J. Xiong, M.F. Lin, J. Wang, S.L. Gaw, K. Parida, P.S. Lee, Wearable all-fabric-based triboelectric generator for water energy harvesting, Adv. Energy Mater. 7 (2017) 1701243.

[15] Y.C. Lai, Y.C. Hsiao, H.M. Wu, Z.L. Wang, Waterproof fabric-based, multifunctional triboelectric nanogenerator for universally harvesting energy from raindrops, wind, and human motions and as self-powered sensors, Adv. Sci. 6 (2019) 1801883.

[16] Z.H. Lin, G. Cheng, L. Lin, S. Lee, Z.L. Wang, Water-solid surface contact electrification and its use for harvesting liquid wave energy, Angew. Chem. Int. Ed. 52 (2013) 1–6.

[17] G. Zhu, Y. Su, P. Bai, J. Chen, Q. Jing, W. Yang, Z.L. Wang, Harvesting water wave energy by asymmetric screening of electrostatic charges on a nanostructured hydrophobic thin-film surface, ACS Nano 8 (2014) 6031–6037.

[18] J. Han, B. Yu, G. Qu, H. Chen, Z. Su, M. Shi, B. Meng, X. Cheng, H. Zhang, Electrification based devices with encapsulated liquid for energy harvesting, multifunctional sensing, and self-powered visualized detection, J. Mater. Chem. 3 (2015) 7382–7388.

[19] D. Choi, S. Lee, S.M. Park, H. Cho, W. Hwang, D.S. Kim, Energy harvesting model of moving water inside a tubular system and its application of a stick-type compact triboelectric nanogenerator, Nano Res. 3 (2015) 7382–7388.

[20] X. Yang, S. Chan, L. Wang, W.A. Daoud, Water tank triboelectric nanogenerator for efficient harvesting of water wave energy over a broad frequency range, Nano Energy 44 (2018) 388–398.

[21] X. Zhang, M. Yu, Z. Ma, H. Ouyang, Y. Zou, S.L. Zhang, H. Niu, X. Pan, M. Xu, Z. Li, Z.L. Wang, Self-powered distributed water level sensors based on liquid-solid triboelectric nanogenerators for ship draft detecting, Adv. Funct. Mater. 29 (2019) 1900327.

[22] L. Liu, Q. Shi, J.S. Ho, C.K. Lee, Study of thin film blue energy harvester based on triboelectric nanogenerator and seashore IoT applications, Nano Energy 66 (2019) 104167.

[23] J.W. Lee, W. Hwang, Theoretical study of micro/nano roughness effect on water-solid triboelectrification with experimental approach, Nano Energy 52 (2018) 315–322.

[24] H. Cho, J. Chung, G. Shin, J.Y. Sim, D.S. Kim, S. Lee, W. Hwang, Toward sustainable output generation of liquid-solid contact triboelectric nanogenerators: the role of hierarchical structures, Nano Energy 56 (2019) 56–64.

[25] J. Chung, D. Heo, B. Kim, S. Lee, Superhydrophobic water-solid contact triboelectric generator by simple spray-on fabrication method, Micromachines 9 (2018) 593.

[26] J.W. Lee, S.M. Kim, T.Y. Kim, U. Khan, S.W. Kim, Water droplet-driven triboelectric nanogenerator with superhydrophobic surfaces, Nano Energy 58 (2019) 579–584.

[27] A.N. Parvez, M.H. Rahaman, H.C. Kim, K.K. Ahn, Optimization of triboelectric energy harvesting from falling water droplet onto wrinkled polydimethylsiloxane-reduced graphene oxide nanocomposite surface, Compos. B Eng. 174 (2019) 106923.

[28] Y. Liu, Y. Zheng, T. Li, D. Wang, F. Zhou, Water-solid triboelectrification with self-repairable surfaces for water-flow energy harvesting, Nano Energy 61 (2019) 454–461.

[29] W. Xu, X. Zhou, C. Hao, H. Zheng, Y. Liu, X. Yan, Z. Yang, M. Leung, X.C. Zeng, R. X. Xu, Z.K. Wang, SLIPS-TENG: robust triboelectric nanogenerator with optical and charge transparency using a slippery interface", Nat. Sci. Rev. 6 (2019) 540–550.

[30] J. Chung, H. Cho, H. Yong, D. Heo, Y.S. Rim, S. Lee, Versatile surface for solid-solid/liquid solid triboelectric nanogenerator based on fluorocarbon liquid infuse surfaces, Sci. Technol. Adv. Mater. 21 (2020) 139–146.

[31] D. Yoo, S.C. Park, S. Lee, J.Y. Sim, I. Song, D. Choi, H. Lim, D.S. Kim, Biomimetic anti-reflective triboelectric nanogenerator for concurrent harvesting of solar and raindrop energies, Nano Energy 57 (2019) 424–431.

[32] Y. Chen, Y. Jie, J. Wang, J. Ma, X. Jia, W. Dou, X. Cao, Triboelectrification on natural rose petal for harvesting environmental mechanical energy, Nano Energy 50 (2018) 441–447.

[33] K.M.T. Negara, I.N.G. Wardana, D. Widhiyanuriyawan, N. Hamidi, Role of the slope on Taro leaf surface to produce electrical energy, IOP Conf. Ser. Mater. Sci. Eng. 494 (2019), 012084.

[34] A. Shahzad, K.R. Wijewardhana, J.K. Song, Contact electrification efficiency dependence on surface energy at the water-solid interface, Appl. Phys. Lett. 113 (2018), 023901.

[35] J. Yu, E. Ma, T. Ma, Harvesting energy from low-frequency excitations through alternate contacts between water and two dielectric materials, Sci. Rep. 7 (2017) 17145.

[36] J. Park, Y. Yang, S.-H. Kwon, Y.S. Kim, Influences of surface and ionic properties on electricity generation of an active transducer driven by water motion, J. Phys. Chem. Lett. 6 (2015) 745–749.

[37] J. Park, S. Ong, C.H. Shin, Y.Y. Yang, S.A.L. Weber, E. Sim, Y.S. Kim, Ion specificity on electric energy generated by flowing water droplets, Angew. Chem. Int. Ed. 57 (2018) 2091–2095.

[38] K.R. Wijewardhana, T.Z. Shen, E.N. Jayaweera, A. Shahzad, J.K. Song, Hybrid nanogenerator and enhancement of water-solid contact electrification using triboelectric charge supplier, Energy 52 (2018) 402–407.

[39] S. Jang, M. La, S. Cho, Y. Yun, J.H. Choi, Y. Ra, S.J. Park, D. Choi, Monocharged electret-based liquid-solid interacting triboelectric nanogenerator for its boosted electrical output performance, Nano Energy 70 (2020) 104541.

[40] L.E. Helseth, Electrical energy harvesting from water droplets passing a hydrophobic polymer with a metal film on its back side, J. Electrost. 81 (2016) 64–70.

[41] L. Yang, Y. Wang, Y. Gao, W. Zhang, Z. Zhao, Robust working mechanism of water droplet-driven triboelectric nanogenerator: triboelectric output versus dynamic motion of water droplet, Adv. Mat. Interfaces 6 (2019) 1901547.

[42] L.E. Helseth, H.Z. Wen, Evaluation of energy generation potential of rain cells, Energy 119 (2017) 472–482.

[43] L.E. Helseth, X.D. Guo, Contact electrification and energy harvesting using periodically contacted and squeezed water droplets, Langmuir 31 (2015) 3269–3276.

[44] J. Ding, W.Q. Tao, S.K. Fang, Study of vibrational droplet triboelectric nanogenerator on structural and operational parameters, Nano Energy 70 (2020) 104473.

[45] Y. Sun, X. Huang, S. Soh, Using the gravitational energy of water to generate power by separation of charge at interfaces, Chem. Sci. 6 (2015) 3347–3353.

[46] L.E. Helseth, X.D. Guo, Hydrophobic polymer covered by a grating electrode for converting the mechanical energy of water droplets into electrical energy, Smart Mater. Struct. 25 (2016), 045007.

[47] B.K. Yun, H.S. Kim, Y.J. Ko, G. Murillo, J.H. Jung, Interdigital electrode based triboelectric nanogenerator for effective energy harvesting from water, Nano Energy 36 (2017) 233–240.
[48] K.R. Wijewardhana, T.Z. Shen, J.K. Song, Energy harvesting using air bubbles on hydrophobic surfaces containing embedded charges, Appl. Energy 206 (2017) 432–438.
[49] K.R. Wijewardhana, T.K. Ekanayaka, E.N. Jayaweera, A. Shahzad, J.K. Song, Integration of multiple bubble motion active transducers for improving energy-harvesting efficiency, Energy 160 (2018) 648–653.
[50] J. Nie, Z. Wang, Z. Ren, S. Li, X. Chen, Z.L. Wang, Power generation from the interaction of a liquid droplet and a liquid membrane, Nat. Commun. 10 (2019) 2264.
[51] Y. Wang, Y. Yang, Superhydrophobic surfaces-based redox-induced electricity from water droplets for self-powered wearable electronics, Nano Energy 56 (2019) 547–554.
[52] D. Choi, H. Lee, D.J. Im, I.S. Kang, G. Lim, D.S. Kim, K.H. Kang, Spontaneous electrical charging of droplets by conventional pipetting, Sci. Rep. 3 (2013) 2037.
[53] Y. Song, B. Xu, Y. Yuan, H. Xu, D. Li, Coalescence of a water drop with an air-liquid interface: electric current generation and critical micelle concentration (CMC) sensing, ACS Appl. Mater. Interfaces 11 (2019) 16981–16990.
[54] P. Jiang, L. Zhang, H. Guo, C. Chen, C. Wu, S. Zhang, Z.L. Wang, Signal output of triboelectric nanogenerator at oil-water-solid multiphase interfaces and its application for dual-signal chemical sensing, Adv. Mater. 31 (2019) 1902793.
[55] Q. Shi, H. Wang, T. Wang, C.K. Lee, Self-powered liquid triboelectric microfluidic sensor for pressure sensing and finger motion monitoring applications, Nano Energy 30 (2016) 450–459.
[56] G. Chen, X. Liu, S. Li, M. Dong, D. Jiang, A droplet energy harvesting and actuation system for self-powered digital microfluidics, Lab Chip 18 (2018) 1026–1034.
[57] Y. Su, X. Wen, G. Zhu, J. Yang, J. Chen, P. Bai, Z. Wu, Y. Jiang, Z.L. Wang, Hybrid triboelectric nanogenerator for harvesting water wave energy and as a self-powered distress signal emitter, Nano Energy 9 (2014) 186–195.
[58] J. Wang, H. Zhang, X. Xie, M. Gao, W. Yang, Y. Lin, Water energy harvesting and self-powered visible light communication based on triboelectric nanogenerator, Energy Technol. 6 (2018) 1929–1934.
[59] J. Wang, H. Wang, X. Li, Y. Zi, Self-powered electrowetting optical switch driven by a triboelectric nanogenerator for wireless sensing, Nano Energy 66 (2019) 104140.
[60] K. Zhao, Z.L. Wang, Y. Yang, Self-powered wireless smart sensor node enabled by an ultrastable, highly efficient and superhydrophobic-surface-based triboelectric nanogenerator, ACS Nano 10 (2016) 9044–9052.
[61] K. Zhang, Y. Wang, Y. Yang, Structure design and performance of hybridized nanogenerators, Adv. Funct. Mater. 29 (2019) 1806435.
[62] C.P. Vo, M. Shahriar, C.D. Le, K.K. Ahn, Mechanically active transducing element based on solid-liquid triboelectric nanogenerator for self-powered sensing, Int. J. Precision Eng. Manuf.-Green Technol. 6 (2019) 741–749.
[63] C. Chen, Z. Wen, A. Wei, X. Xie, N. Zhai, X. Wei, M. Peng, Y. Liu, X. Sun, J.T. W. Yeow, Self-powered on-line ion concentration monitor in water transportation driven by triboelectric nanogenerator, Nano Energy 62 (2019) 442–448.
[64] W. Zhang, P. Wang, K. Sun, C. Wang, D. Diao, Intelligently detection and identifying liquids leakage combining triboelectric nanogenerator based self-powered sensor with machine learning, Nano Energy 56 (2019) 277–285.
[65] A.Z. Stetten, D.S. Golovko, S.A.L. Weber, H.J. Butt, Slide-electrification: charging of surfaces by moving water drops, Soft Matter 15 (2019) 8667–8679.
[66] J.K. Beattie, The intrinsic charge on hydrophobic microfluidic substrates, Lab Chip 6 (2006) 1409–1411.
[67] K.N. Kudin, R. Car, Why are water-hydrophobic interfaces charged, J. Am. Chem. Soc. 130 (2007) 3915–3919.
[68] M.D. Baer, I.F.W. Kuo, D.J. Tobias, C.J. Mundy, Towards a unified picture of the water self-ions at air-water interface: a density functional theory perspective, J. Phys. Chem. B 118 (2014) 8364–8372.
[69] S. Strazdaite, J. Versluis, H.J. Bakker, Water orientation at hydrophobic interfaces, J. Chem. Phys. 143 (2015), 084708.
[70] K. Yatsuzuka, Y. Mizuno, K. Asano, Electrification phenomena of pure water droplets dripping and sliding on a polymer surface, J. Electrost. 32 (1994) 157–171.
[71] J. Nie, Z. Ren, L. Xu, S. Lin, F. Zhan, X. Chen, Z.L. Wang, Probing contact-electrification-induced electron and ion transfers at a liquid-solid interface, Adv. Mater. 32 (2020) 1905696.
[72] S. Li, Y. Fan, H. Chen, J. Nie, X. Tao, J. Zhang, X. Chen, E. Fu, Z.L. Wang, Manipulating the triboelectric surface charge density of polymers by low-energy helium ion irradiation/implantation, Energy Environ. Sci. 13 (2020) 896–907.
[73] L.E. Helseth, The influence of microscale surface roughness on water-droplet contact electrification, Langmuir 35 (2019) 8268–8275.
[74] T. Preočanin, A. Selmani, P. Lindqvist-Reis, F. Heberling, N. Kallay, J. Lützenkirchen, Surface charge at Teflon/aqueous solution of potassium chloride interfaces, Colloids Surf., A 412 (2012) 120–128.
[75] Q.A. Pankhurst, J. Connolly, S.K. Jones, J. Dobson, Applications of magnetic nanoparticles in biomedicine, J. Phys. D Appl. Phys. 36 (2003) R167.
[76] L.E. Helseth, Optical sensor for detecting colloidal phase transitions induced by magnetic fields, J. Phys. D Appl. Phys. 42 (2009) 105005.
[77] L.E. Helseth, Paramagnetic particles as sensitive force detectors in liquids, J. Phys. D Appl. Phys. 40 (2007) 3030.

Lars Egil Helseth obtained his PhD from the University of Oslo (Norway) in 2002. He was a postdoc at Max Planck Institute for Colloids and Interfaces (Golm, Germany) and later at Florida State University (Tallahassee, USA), before becoming an Assistant Professor at the Nanyang Technological University (Singapore) in 2005. In 2008 he was appointed Professor at the Department of Physics and Technology, University of Bergen (Norway). His fields of interests lie within electromagnetism, with particular emphasis on sensors development and energy harvesting.